Oscillating epidemics in a dynamic network model: stochastic and mean-field analysis

Article (Accepted Version)

J. Math. Biol.
DOI 10.1007/s00285-015-0902-3

Mathematical Biology

Oscillating epidemics in a dynamic network model: stochastic and mean-field analysis

András Szabó-Solticzky[1,2] · Luc Berthouze[3] · Istvan Z. Kiss[4] · Péter L. Simon[1,2]

Received: 17 October 2014 / Revised: 19 May 2015

Abstract An adaptive network model using SIS epidemic propagation with link-type-dependent link activation and deletion is considered. Bifurcation analysis of the pairwise ODE approximation and the network-based stochastic simulation is carried out, showing that three typical behaviours may occur; namely, oscillations can be observed besides disease-free or endemic steady states. The oscillatory behaviour in the stochastic simulations is studied using Fourier analysis, as well as through analysing the exact master equations of the stochastic model. By going beyond simply comparing simulation results to mean-field models, our approach yields deeper insights into the observed phenomena and help better understand and map out the limitations of mean-field models.

Keywords SIS epidemic · Pairwise model · Dynamic network · Oscillation

Mathematics Subject Classification 05C82 · 60J28 · 92D30 · 34C23

✉ Istvan Z. Kiss
i.z.kiss@sussex.ac.uk

1 Institute of Mathematics, Eötvös Loránd University, Budapest, Hungary

2 Numerical Analysis and Large Networks Research Group, Hungarian Academy of Sciences, Budapest, Hungary

3 Centre for Computational Neuroscience and Robotics, University of Sussex, Falmer, Brighton BN1 9QH, UK

4 Department of Mathematics, School of Mathematical and Physical Sciences, University of Sussex, Falmer, Brighton BN1 9QH, UK

Published online: 11 June 2015

1 Introduction

Network-related research has recently seen rapid developments in the area of dynamic or adaptive networks (Gross and Blasius 2008; Juher et al. 2013; Marceau et al. 2010; Shaw and Schwartz 2008). This is partly motivated by empirical observations showing that in many instances dynamical processes on networks co-evolve with the dynamics of the networks themselves (Gross and Blasius 2008). This in turn leads to a wider spectrum of possible behaviours, such as bistability and oscillations, when compared to static network models. Examples of dynamic/adaptive networks are abundant and link or contact fluidity is a common feature of both technological and social networks. In this paper, we study dynamic networks in which the timescales of the two processes are comparable, and we do this in the context of a basic but fundamental model of disease transmission.

Early work in the area of dynamic networks, which then gave rise to many model improvements and extensions, concentrated on epidemic models with 'smart' rewiring, where infection transmitting links are replaced by non-risky ones, with a link-conserving network dynamics. The most widely used approach to study such systems is the development of mean-field models, such as pairwise (Gross et al. 2006; Kiss et al. 2012) and effective-degree models (Marceau et al. 2010; Taylor et al. 2012), which usually manage to capture and characterise such processes to a good level of detail. For example, using pairwise models and simulations, Gross et al. (2006) showed that rapid rewiring can stop disease transmission, while Marceau et al. (2010) used the effective-degree model, i.e., an improved compartmental model formalism, to obtain better predictions and shed more light on the evolution of the network structure. Furthermore, Juher et al. (2013) fine-tuned the bifurcation analysis of the model originally proposed in Gross et al. (2006) to distinguish between two extinction scenarios and to provide an analytical condition for the occurrence of a bistability region.

Recognising the idealised nature of link-number-conserving smart rewiring, various relaxations to these models were introduced. For example, Kiss et al. (2012) and Szabó et al. (2012) proposed a number of dynamic network models including random link activation-deletion with and without constraints, as well a model that considered non-link preserving link-type-dependent activation and deletion. Taylor et al. (2012) used the effective degree formalism to analyse a similar random link activation-deletion model and highlighted the potential power of link deletion in eradicating epidemics. Recently Rogers et al. (2012) introduced an SIRS model where random link activation-deletion is combined with 'smart' rewiring. They studied the resulting stochastic model at the level of singles and pairs as well as its deterministic limit, i.e., pairwise or pair-based models. Other node dynamics, such as the voter model, have also been extensively studied on adaptive networks; see Demirel et al. (2014) and Sayama et al. (2013) for a review.

An overview of the above studies highlights some important modelling and analysis challenges. On the model development front it is clear that many models are still very idealised and small steps toward increasing model realism can quickly lead to a disproportionate increase in model complexity. The agreement between mean-field and stochastic models is very much model- and parameter-dependent with potentially large parameter regions in which agreement can be either good or poor. This is particularly

the case when oscillations are encountered or expected (Gross and Kevrekidis 2008). Indeed, despite being observed in Gross et al. (2006), their existence has remained controversial because very large systems need to be simulated for stable oscillations to be observed for extended periods of time. When oscillatory behaviour is expected, there are only few results in an epidemic context, see Zhou et al. (2012) for example. Studies of epidemic propagation on adaptive networks have not focused much on characterising oscillatory behaviour in simulations and there is no widely accepted analytical framework for this as of yet. Another major drawback in the analysis of dynamic networks is that even when mean-field models perform well, these only provide limited insight about the structure and evolution of the network.

In this paper, we set out to address some of these issues and make important steps towards a more satisfactory treatment and analysis of dynamic network models, along with a better use and integration of various mathematical methods and techniques that can be employed. To this end we propose a dynamic network model using SIS epidemic propagation with link-type-dependent link activation and deletion. We provide model analysis based on both (a) mean-field and (b) purely network-based stochastic simulation model. The latter is carried out using Fourier analysis, as well as through analysing the exact stochastic model in terms of the master equations.

The paper is structured as follows. The link-type-dependent activation-deletion model is formulated in Sect. 2. Then the pairwise ODE approximation augmented by terms accounting for preferential link cutting and creation is analysed in Sect. 3. Guided by the bifurcation analysis of the mean-field model, in Sect. 4, we carry out a detailed study of the stochastic model and analyse the agreement between the stochastic and pairwise model. Oscillations are observed both in the mean-field approximation and the stochastic network simulation. In Sect. 5, the emergence of oscillations in the stochastic model is explained and we discuss how the oscillatory behaviour in the epidemic translates to changes in network structure. Furthermore, we consider the exact master equation for an idealised dynamic network model in order to shed light on why and how oscillations can arise. The paper concludes with the discussion of our findings and further outstanding questions.

2 Model formulation

In this paper SIS (susceptible-infectious/infected-susceptible) epidemic propagation is considered on an adaptive network with link-type-dependent link activation and deletion. Specifically, the model incorporates the following independent Poisson processes:

- **Infection**: Infection is transmitted across each contact between an S and an I node, or (SI) link, at rate τ,
- **Recovery**: Each I node recovers at rate γ, and this is independent of the network,
- **Link activation**: A non-existing link between a node of type A and another of type B is activated at rate α_{AB}, with $A, B \in \{S, I\}$,
- **Link deletion**: An existing link between a node of type A and another of type B is terminated at rate ω_{AB}, with $A, B \in \{S, I\}$.

We note that once a link type is chosen, the activation or deletion of such a link is done at random. Our model is significantly different from the widely used setup of

'smart' rewiring (Gross and Blasius 2008), where the S nodes have full knowledge of the states of all other nodes and choose to minimise their exposure to the epidemic by cutting links to I neighbours and immediately rewiring to a randomly chosen S node. This also conserves the number of links in the network and can make the analysis more tractable, by reducing the complexity of the model.

Here, we set out to explore and explain as fully as possible the complete spectrum of system behaviours, including classical bifurcation analysis at system level, e.g., die-out, endemic equilibria or oscillations. In order to do this, we will employ (a) full network-based Monte Carlo simulations, and (b) an exact Master Equation formulation for small networks. Regarding the rewiring parameters we focus on the scenario

$$\alpha_{SI} = \alpha_{II} = 0 \quad \text{and} \quad \alpha_{SS} \neq 0, \quad \text{and} \quad \omega_{II} = \omega_{SS} = 0 \quad \text{and} \quad \omega_{SI} \neq 0,$$

which is motivated by the same practical considerations as those used in 'smart' rewiring—where nodes aim to minimise the risk of becoming infected while maintaining their connectivity to the network. We note that the case of random link creation and deletion which decouples the two processes has been analysed in Kiss et al. (2012), where it was conjectured that no oscillations can arise. Moreover, numerical experimentation with several parameter combinations suggests that the scenario above seems to be the simplest that gives rise to oscillations.

3 Simple pairwise model: bifurcation analysis

We start by formulating the pairwise model for the expected values of the node and pair numbers. As was shown in Kiss et al. (2012), this gives rise to

$$\dot{[I]} = \tau[SI] - \gamma[I], \tag{1}$$

$$\dot{[SI]} = \gamma([II] - [SI]) + \tau([SSI] - [ISI] - [SI]) - \omega_{SI}[SI], \tag{2}$$

$$\dot{[II]} = -2\gamma[II] + 2\tau([ISI] + [SI]), \tag{3}$$

$$\dot{[SS]} = 2\gamma[SI] - 2\tau[SSI] + \alpha_{SS}([S]([S] - 1) - [SS]), \tag{4}$$

where, based on Keeling (1999), $[A]$ is the expected value of the number of nodes in state A; $[AB] = \sum_{ij} A_i B_j g_{ij}$, where $G = (g_{ij})_{i,j=1,2,\ldots,N}$ is the adjacency matrix of the network, such that $g_{ij} = g_{ji}$, $g_{ii} = 0$ and $g_{ij} = g_{ji} = 1$ if nodes i and j are connected and zero otherwise. Furthermore, A_i is 1 if node i is in state A and similarly for B_j with $A, B \in \{S, I\}$. This then implies that (SS) and (II) links are doubly counted and that $[SI] = [IS]$. The model is not non-dimensionalised or scaled and all rate have units of $\frac{1}{Time}$. Furthermore, we note that $([S]([S] - 1) - [SS])$ is simply equivalent to the doubly counted expected number of (SS) links which are not yet connected. From the model it follows that $[S]+[I] = N$ and $[SS]+2[SI]+[II] = \langle k \rangle N$, where $\langle k \rangle$ is the time-dependent average degree and N is the number of nodes in the network. The closures of the triples in terms of singles and pairs require the expected average degree of S nodes. This is given by

$$k_S(t) = \frac{[SS] + [SI]}{[S]}. \tag{5}$$

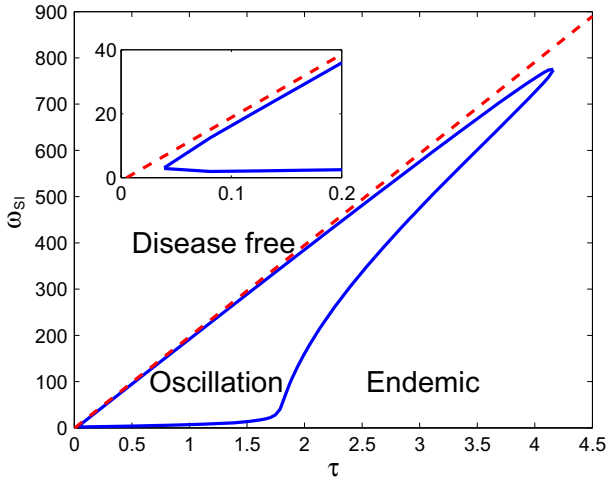

Fig. 1 Bifurcation diagram for the pairwise ODE model in the (τ, ω_{SI}) parameter space for $N = 200$, $\gamma = 1$ and $\alpha_{SS} = 0.04$. The transcritical bifurcation occurs along the *dashed line*, and the Hopf bifurcation occurs along the perimeter of the island

The well-known closures (Keeling 1999) are used, namely

$$[SSI] = \frac{(k_S - 1)[SS][SI]}{k_S[S]} \quad \text{and} \quad [ISI] = \frac{(k_S - 1)[SI][SI]}{k_S[S]}. \tag{6}$$

Upon applying these closures, a self-consistent system with 4 ODEs is obtained. This can be analysed using classical bifurcation theory techniques. The system admits two equilibria: (a) a disease-free equilibrium $([S], [I], [SI], [II], [SS]) = (N, 0, 0, 0, N(N-1))$ and (b) an endemic equilibrium which cannot be explicitly given due to being the solution of a quartic equation.

The linearisation around the disease-free steady state gives rise to a 4×4 Jacobian, the eigenvalues of which can be determined explicitly, see Appendix A. As shown, two of the eigenvalues are always negative and the remaining two have negative real part if and only if

$$\omega_{SI} > \tau(N-2) - \gamma. \tag{7}$$

According to the next two propositions a transcritical bifurcation occurs along the line $\omega_{SI} = \tau(N-2) - \gamma$, see Fig. 1. Namely, it will be shown that the disease-free steady state loses its stability there and an endemic steady state appears.

Proposition 1 *The disease-free steady state is asymptotically stable if and only if* $\omega_{SI} > \tau(N-2) - \gamma$.

We note that numerical results suggest that in fact the disease-free steady state is globally asymptotically stable. As mentioned above the endemic steady state is the solution of a quartic equation, see Appendix A for its detailed derivation. The analysis of this equation leads to the following proposition concerning the existence of the endemic steady state.

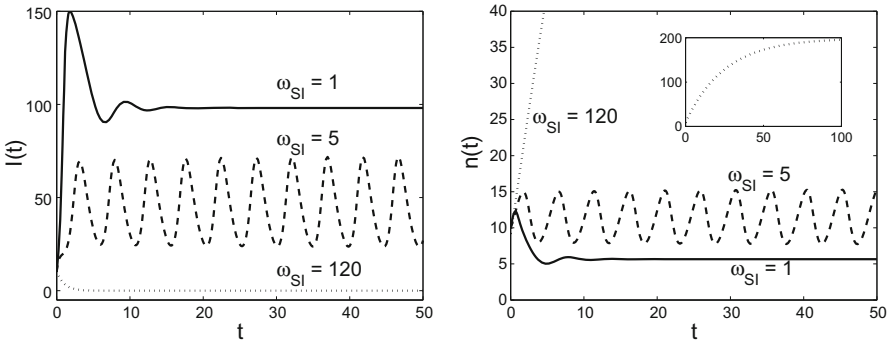

Fig. 2 Time dependence of prevalence (*left panel*) and average degree (*right panel*) in the pairwise ODE model for $\omega_{SI} = 1$ (*continuous*), $\omega_{SI} = 5$ (*dashed*) and for $\omega_{SI} = 120$ (*dotted*). The inset in the right panel shows the time dependence of the average degree for $\omega_{SI} = 120$. The values of the other parameters are fixed at $\tau = 0.5$, $N = 200$, $\gamma = 1$ and $\alpha_{SS} = 0.04$

Proposition 2 *If $x \in (0, N)$ is a root of polynomial (15) given in Appendix A, then the system has an endemic steady state, the coordinates of which can be given as*

$$[S]_{ss} = x, \quad [I]_{ss} = N - x, \quad [SI]_{ss} = \frac{\gamma}{\tau}(N - x),$$
$$[SS]_{ss} = x(x-1) - 2\frac{\omega_{SI}\gamma}{\alpha_{SS}\tau}(N - x), \quad [II]_{ss} = \frac{\gamma(N-x)^2}{\tau x} + \frac{(N-x)[SS]_{ss}}{[SS]_{ss} + [SI]_{ss}}.$$

An extensive numerical study has shown that below the line of transcritical bifurcation there is a unique endemic steady state, i.e., the polynomial has a single root providing a biologically plausible steady state, where the values of all singles and pairs are positive. For the endemic steady state, the coefficients of the characteristic polynomial can only be determined numerically but this does not prevent from determining where the Hopf bifurcation arises (see Appendix A for details). The Hopf bifurcation points form a set as depicted by the curve, i.e., the perimeter of the island, in Fig. 1. The results of the numerical study show that within the Hopf island the mean-field model exhibits stable oscillations. The region below the transcritical bifurcation line and outside the Hopf island is where the endemic equilibrium is stable. It is important to note that the system-level analysis can be complemented by the observation that the expected average degree displays a behaviour similar to that of the expected number of infected, as illustrated by Fig. 2.

A careful analysis of the plots based on the mean-field model allows to make the following important remarks. Edge deletion and creation acts on very different edge numbers. The creation of (SS) links acts on a set of edges with cardinality of $O(N^2)$, while the infection process and the deletion of (SI) edges act on a set of edges whose number scales as $\langle k \rangle [I]$. In order to ensure that all processes act in a comparable way, rates need to be adjusted accordingly, e.g., smaller values for the α_{SS} rate compared to the rate of cutting SI links, ω_{SI}. The conclusion of the analysis of the pairwise model is that the system can exhibit three different behaviours: (a) disease-free steady state, (b) endemic steady state, and (c) oscillations. Moreover, the

bifurcation boundaries separating these states can be analytically determined and for given parameter values numerically computed. This analysis offers a valuable insight into the possible behaviours that can be expected from the full network simulation.

4 Characterisation of the full network-based stochastic model

With the insight gained from the analysis of the mean-field model, we set out to investigate and map out the spectrum of behaviour directly from the network-based stochastic simulation, that is, the analogue of the continuous-time Markov Chain corresponding to the process. The simulation is based on a careful and continuous book keeping of all possible single events, i.e., infection across a link, recovery of a node, activation or deletion of a link. Based on a 'current' state all possible events and their rates are computed, or these are known based on a previous state supplemented by necessary changes induced by the most recent event. The time to the next event is chosen from an exponential distribution whose parameter is the total rate. Then, an event is chosen at random but proportionally to its rate. This is very much in line with the Gillespie algorithm (Gillespie 1976a, b). Given that all existing and non-existing links need to be accounted for, the algorithm which includes the storage, update and referencing back and forth between rates and events becomes more complex, concretely, from order N to order N^2 complexity. We wish to emphasise that the $\alpha_{SS}([S]([S]-1)-[SS])$ term in Eq. 4 implies that in the simulation, one either considers each potential (SS) link twice and attempts to create each at rate α_{SS} or considers every such link once but attempts to create it at rate $2\alpha_{SS}$. This will ensure that the double counting induced by the pairwise model is correctly translated into the simulation. For the deletion of (SI) links there is no such problem and the relation between mean-field model and simulation is straightforward.

Simulations were run in which τ and ω were systematically sampled in the interval $[0.05, 20]$ and $[0.05, 13]$ respectively. For each configuration pair, 100 simulations were run with $N = 200$, $\gamma = 1$, $\alpha_{SS} = 0.04$, $T_{max} = 1320$ and resampling rate 0.01, yielding 132,000 time points per run. The starting networks are Erdős-Rényi random networks with $\langle k \rangle = 10$.

4.1 Simulation results

Simulations show that the system exhibits exactly those three regimes that were predicted by the pair-based mean-field model. Fig. 3 shows representative samples of the system's behaviour in the endemic and oscillatory regimes. As we cannot expect sharp bifurcation boundaries between regimes in the stochastic model, we now propose empirical definitions for the boundaries of the different regimes.

4.1.1 Boundary of the disease-free regime

For each configuration pair (τ, ω), we determined the proportion of realizations in which the epidemic died out. Figure 4 shows a representative example (at $\tau = 12$) when ω is varied over the whole range $[0.05, 13]$ and all other parameters are kept constant.

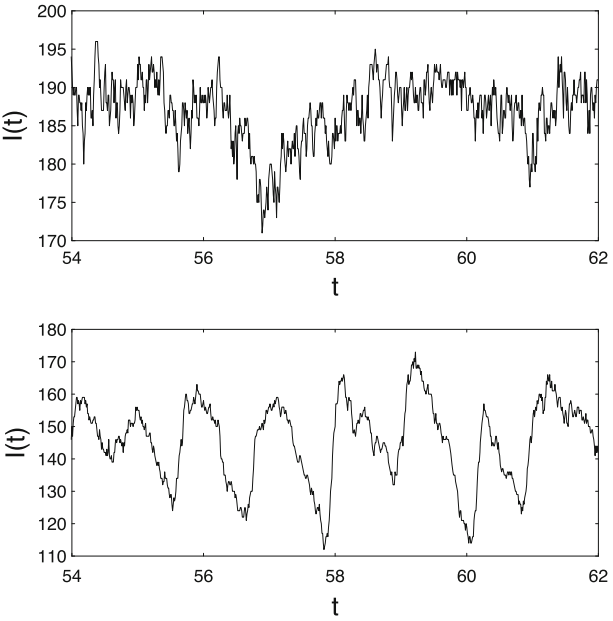

Fig. 3 Sample time series (800 time points) of the number of infected nodes in the endemic regime (*top panel*, $\omega_{SI} = 0.5$) and oscillatory regime (*bottom panel*, $\omega_{SI} = 4.0$). These samples were randomly chosen from one of 100 realisations using the following parameters: $N = 200$, $\tau = 12$, $\gamma = 1$, $\alpha_{SS} = 0.04$

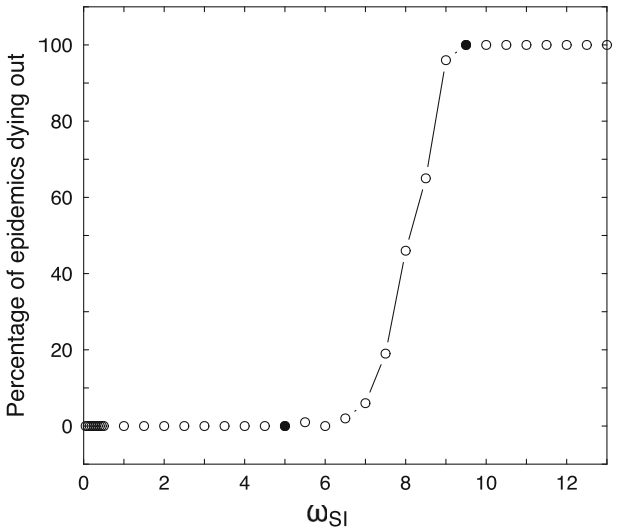

Fig. 4 Percentage of epidemics dying out before $T_{max} = 1320$ with $\tau = 12$ and ω_{SI} (*horizontal axis*) varying between 0.05 and 13. This percentage is calculated out of 100 realisations using the following parameters: $N = 200$, $\tau = 12$, $\gamma = 1$, and $\alpha_{SS} = 0.04$. The values of ω_{SI} below which no realisations die out and above which all realisations die out define two possible boundaries for the disease-free regime and are shown by *solid circles*

The figure shows a sharp increase in the proportion of realisations in which epidemics die out such that two potential boundaries can be defined: one which corresponds to the parameter up to which none of the realisations die out, and one in which all realisations die out. These two boundaries delimit a strip that can be considered as the bifurcation boundary of the disease-free regime. The width of this strip is shown by the grey-shaded area in Fig. 6.

4.1.2 Boundary of the oscillating regime

For those realizations that did not die out (over the entire duration of the run, i.e., $T_{max} = 1320$), evidence for oscillatory behaviour was assessed through a rigorous statistical analysis of the power spectrum of the time series of the number of infected nodes. The spectral estimation procedure was based on weighted periodogram estimates. The data was split into non overlapping segments, each containing 2^{13} points and the periodograms were calculated from application of discrete Fourier transforms (DFT). As application of DFT requires stationarity of the time series, transients in the time series were removed using the following procedure. After confirming pseudo-stationarity of the last 2^{13} points (one segment) of the time series, their mean and standard deviation were computed. A running average (low-pass filter) of the entire time series was then applied and the first time point after which all subsequent time points of the filtered time series stayed within 5 % of the standard deviation of the mean of the last segment was selected as the starting point of the transient-free time series. Only those time series with at least 2^{15} time points were kept for analysis, allowing for a theoretical minimum of 4 segments to be included in the spectral estimation. In practice, provided transient-free data could be found, all parameter configuration yielded no less than 13 segments with most configurations yielding 1300 segments. Presence of a non-trivial oscillatory component in the signal was assessed by the presence of statistically significant power at a non-zero frequency peak in the power spectrum, with confidence intervals for the spectral estimates obtained as per the framework of Halliday et al. (1995). The non-zero frequency constraint is required because, as mentioned in Rogers et al. (2012), time series in which the spectrum is dominated by the zero mode can be difficult to distinguish from pure white noise. To identify the boundaries of the oscillatory regime, power and frequency of the main peak of the power spectrum were recorded for all configuration pairs studied above. Figure 5 shows a representative example (at $\tau = 12$ but see Fig. 6 as well for an overall picture of the peak frequency) when ω is varied over the whole range [0.05, 13] and all other parameters are kept constant. The figure reveals a pattern in which, with increasing ω, there is initially a rapid increase in the power at the frequency of peak power, however, this frequency is small enough that the signal may not be considered oscillatory. This phase is followed by a clear increase in the frequency at peak power followed by a plateau with near constant power until ω reaches the boundary of the disease-free regime. As illustrated by Fig. 6, with increasing τ, the peak frequency can decrease to near zero levels such that the system briefly returns to the endemic regime. This is consistent with the result from the theoretical bifurcation diagram which shows a narrow strip of endemic regime between oscillatory regime and disease-free regime (e.g., see $\tau = 4$ and $\omega \approx 780$ in Fig. 1). Thresholding of the frequency at peak power makes

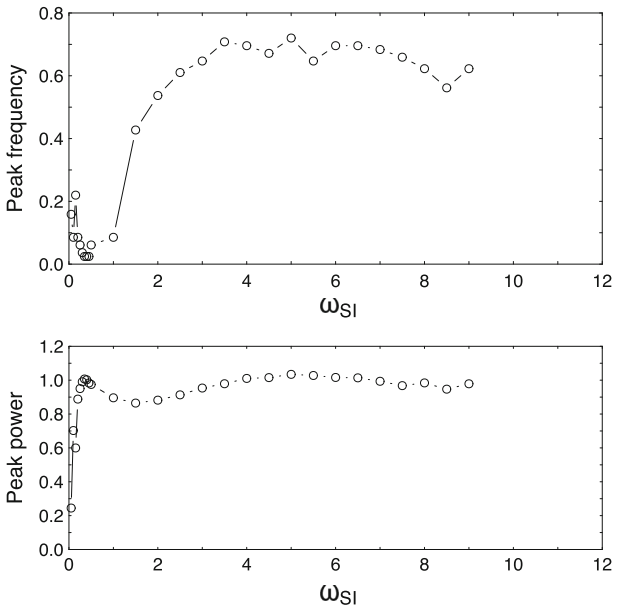

Fig. 5 Frequency at peak power and peak power for $\tau = 12$ and ω_{SI} (*horizontal axis*) varying between 0.05 and 13. The absence of data for $\omega_{SI} > 9$ reflects the fact that the disease-free regime has been reached, see Fig. 4. Thresholding of peak frequency at non-zero value makes it possible to define a boundary for the oscillatory regime

it possible to define a boundary for the oscillatory regime. This is a soft boundary in that there is no *a priori* basis for deciding a set level.

4.1.3 Bifurcation diagram in the (τ, ω) *plane*

Figure 6 shows the bifurcation "curves" and the domains of the three different behaviours. Qualitatively, the plot confirms the prediction of the theoretical model with a bounded oscillatory domain abbuting the disease-free domain (here represented by a zero-disease boundary defined by all realizations dying out before T_{max}) at low values of τ ($\tau < 10$) and showing a narrow strip of remaining endemic regime at higher τ values ($\tau > 10$). When considering the stricter boundary, one observes an overlap between the disease-free regime and the oscillatory regime. Practically, this is characterised by time series of the number of infected nodes showing a large seesaw pattern of a long continuous decrease followed by a very rapid and large increase.

4.2 Comparison of pairwise and simulation models

4.2.1 Comparison of the time evolution

In Fig. 7, we show direct comparisons between the outcome from stochastic simulation and results from the pairwise model. We illustrate the two typical behaviours in the

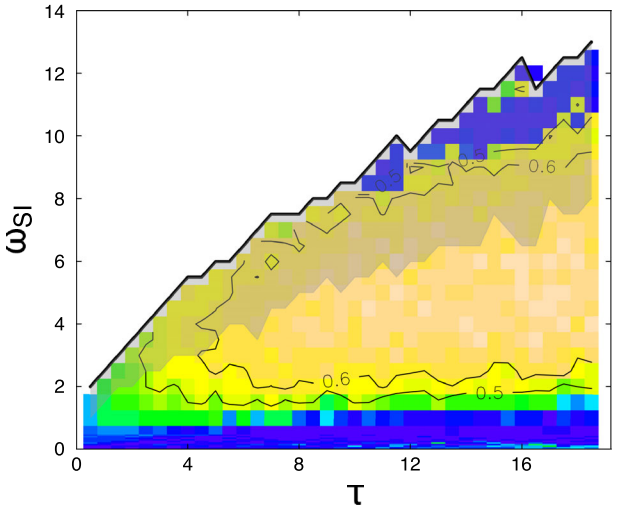

Fig. 6 Equivalent of the bifurcation diagram for the stochastic model in the (τ, ω_{SI}) parameter space for $N = 200$, $\gamma = 1$, $\alpha_{SS} = 0.04$. Identification of the oscillatory regime relies on the value of the frequency of peak power. Two potential boundaries are provided in the form of iso-lines at values 0.5 and 0.6. Peak frequency was ≈0.75 (*orange colour*). Near zero frequencies are shown in *dark blue*. These boundaries are qualitatively consistent with those observed in the theoretical model. The *thick black line* shows one boundary for the disease-free regime determined as the value of ω_{SI} above which all realisations die out. The *bottom* boundary of the shaded area represents an alternative boundary determined as the value of ω_{SI} under which no realisations die out (colour figure online)

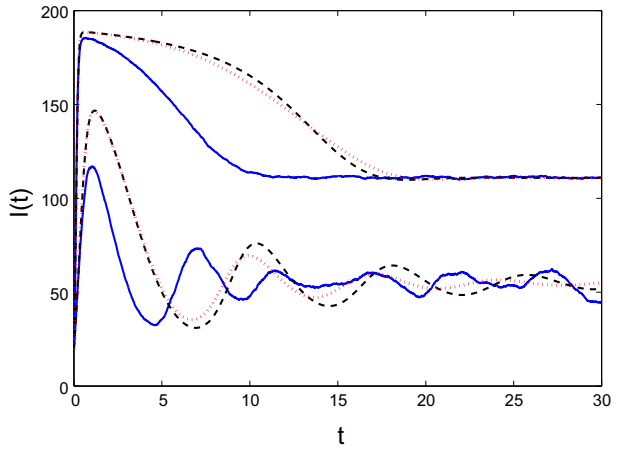

Fig. 7 Comparison of the time evolution of prevalence in a network with $N = 200$ nodes obtained from the average of 500 simulations (*continuous blue curves*), from the simple pairwise model (1)–(4) (*dashed black curves*) and from the compact pairwise model (*dotted red curves*). The parameter values for the endemic case (*upper curves*) are $\alpha_{SS} = 0.01$, $\omega_{SI} = 0.7$, $\gamma = 1$, $\tau = 2$ and those yielding the oscillating solutions (*lower curves*) are $\alpha_{SS} = 0.01$, $\omega_{SI} = 1.5$, $\gamma = 1$, $\tau = 0.8$. For the oscillating case only simulations which did not die out until $t = 20$ were taken into account (colour figure online)

presence of infection. As shown by the figure, there is reasonable agreement. Comparing oscillations is particularly difficult since small variations and de-phasing due to stochastic effects will result in the loss of the oscillatory behaviour when averaging over many individual realisations. An important issue that may lead to disagreement is the heterogeneity of the degree distribution that is created by the process itself. Epidemics on networks with heterogeneous degrees can be described by heterogeneous mean field models (Eames and Keeling 2002). However, the number of equations in this type of models is of order $O(N^2)$ since the degree in a dynamic network can, in principle, vary between 0 and $N-1$, where N is the number of nodes in the network. As a compromise between keeping degree heterogeneity and having a tractable system of ODEs, so-called compact pairwise models have been introduced (House and Keeling 2011). The variables of this model are $[S_k]$ and $[I_k]$ representing the average number of susceptible and infected nodes of degree k, respectively, and, the average number of pairs $[SI]$, $[SS]$ and $[II]$. The solution of the compact pairwise adapted to the dynamic network case (not presented in detail here) is also compared to simulation, see Fig. 7. One can observe that introducing degree heterogeneity in the model does not improve the agreement significantly. This may be explained by the fact that the main argument for closing triples in the pairwise and compact pairwise models is identical. Namely, both models assume that the states of a susceptible node's neighbours are effectively chosen independently and at random from the pool of available nodes. Typically, it is relatively easy to find many parameter combinations where the agreement is satisfactory to good, especially for the endemic equilibrium. However, in what follows we aim to make a more principled comparison between the two models in the full parameter space.

4.2.2 Comparison between bifurcation diagrams

From a visual inspection of the two bifurcation diagrams in Figs. 1 and 6, it is clear that the overall qualitative features of the model are captured well by both full stochastic and pairwise models. However, there are significant quantitative discrepancies. Most remarkably, the pairwise model significantly overestimates the slope of the transcritical bifurcation curves, effectively prescribing much higher cutting rates than needed in order to curtail an epidemic in the stochastic model. Starting from this crucial observation we comment on some fundamental and perhaps unresolvable differences which are mainly due to the natural limitations of the models. In particular, the transcritical bifurcation curve from the pairwise model requires that the network be fully connected. Hence, this naturally leads to a very high critical ω_{SI} rate, which is required in order to stop the epidemic in a fully connected network. There is a subtle point to be made here. Controlling the epidemic on a fully connected network via link cutting will, in most cases, require a punishingly high rate. This can take the network's average degree to very low values. This does not create a problem for the pairwise model in which the infection will be able to recover from very small levels of prevalence and spare networks. However, in such cases, in the stochastic model, there is a high probability that at low prevalence and sparsely connected network, the epidemic dies out. This suggests that smaller values of cutting rates are sufficient to yield the disease-free regime.

5 Explanation for the oscillatory behaviour

5.1 Simulation-based tracking

Oscillations within the context of adaptive networks have proved to be difficult to map out, especially directly from simulations. For many oscillatory systems the basic ideas of processes leading to oscillations are relatively simple. Usually, a combination of a positive and negative feedback with a suitable time delay leads to robust oscillations. Taking inspiration from this idea, it is possible to give a heuristic explanation for the appearance of oscillations in this adaptive network. The basic oscillating quantities in our explanation are the prevalence $[I]$ and the average degree $\langle k \rangle$, for which exact differential equations can be written down

$$
\begin{aligned}
[\dot{I}] &= \tau[SI] - \gamma[I], \\
\langle \dot{k} \rangle &= \alpha_{SS}([S]([S]-1) - [SS]) - 2\omega_{SI}[SI].
\end{aligned}
$$

Thus as it can be immediately seen, the direction of change of these quantities is determined by the velocity of the following four processes.

- **A**: Infection with rate $\tau[SI]$,
- **B**: Recovery of I nodes with rate $\gamma[I]$,
- **C**: Creation of SS links with rate $\alpha_{SS}([S]([S]-1) - [SS])$ and
- **D**: SI link deletion with rate $\omega_{SI}[SI]$.

The important stages during the cycle of an oscillation are determined by the strength of process **A** relative to **B** and that of **C** compared to **D**. To explain and visualise this, let us consider an epidemic that is well established and is capable of sustaining oscillations. Let us start from the situation where there are few infected nodes and the epidemic is about to take off, i.e., when process **A** dominates **B** and **C** is stronger than **D**. In this case, the expansion of the epidemic usually is also followed by the network becoming more connected given that the total rate of link cutting is smaller than the total rate of link creation, i.e., $2\omega_{SI}[SI] < \alpha_{SS}([S]([S]-1) - [SS])$. This is expected as the epidemic is just recovering from an excursion where the connectivity of the network was low and the number of susceptible nodes was large. However, as the epidemic grows the balance of processes **C** and **D** changes. Namely, when the epidemic is still strong, the number of susceptible nodes decreases while the link cutting acts on an increasing number of (SI) edges. This reverts the balance of edge cutting and deletion meaning that now $2\omega_{SI}[SI] > \alpha_{SS}([S]([S]-1) - [SS])$. In Fig. 8a, a snapshot at the peak connectivity is shown. At this stage, the epidemic can and will continue to grow, i.e., **A** still dominates **B**. However, close to the highest possible prevalence level, shown in Fig. 8b, the recovery acting on the majority of the nodes and the cutting of occasional (SI) links will outcompete the spread of infection, that is, **B** will be stronger than **A**. The continued loss of links leads to observing the 'segregation' of the network, as shown in Fig. 8c, which amounts to the formation of susceptible and infected node clusters/clumps with occasional between cluster links. At this point, due to the increasing number of susceptible nodes, link creation will start to dominate and the susceptible clusters/clumps will become more densely connected.

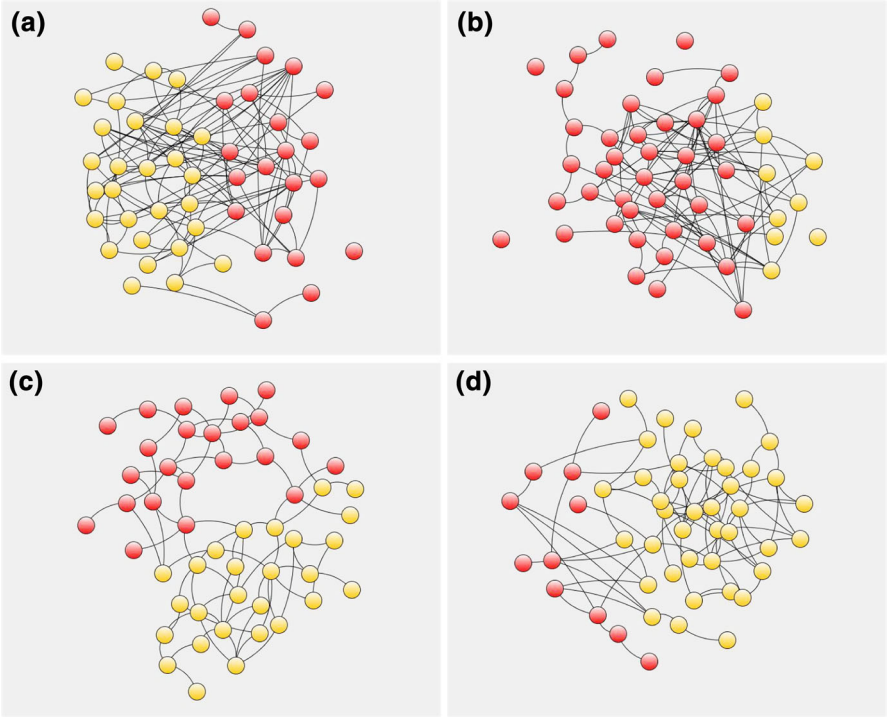

Fig. 8 Temporal snapshots of the main phases of an oscillation cycle are: **a** the growing phase of the epidemic with $\langle k \rangle$ close to its maximum, **b** close to the maximum prevalence and a decreasing average degree, **c** decreasing prevalence with $\langle k \rangle$ close to its minimum and, finally, **d** minimal prevalence but with growing average degree. Parameter values are $N = 50$, $\tau = \gamma = 1$, $\omega_{SI} = 1.3$, $\alpha_{SS} = 0.04$ with all the other activation and deletion rates being equal to zero. Susceptible and infected nodes are represented by *yellow* and *red circles*, respectively (colour figure online)

The survival of the epidemic now simply relies on the few inter-clump links which will allow infection to become re-established in the densely connected susceptible parts of the network, see Fig. 8d. This is often followed by a sudden epidemic expansion, i.e., the dominance of **A** over **B**. This last phase finishes the cycle and the system is back to the growing epidemic stage again as explained at the start of our argument. Summarising, the four stages of the oscillation can be characterised as follows:

1. $\mathbf{A} > \mathbf{B}$, $\mathbf{C} > \mathbf{D}$, $[I]$ increasing, $\langle k \rangle$ increasing,
2. $\mathbf{A} > \mathbf{B}$, $\mathbf{C} < \mathbf{D}$, $[I]$ increasing, $\langle k \rangle$ decreasing,
3. $\mathbf{A} < \mathbf{B}$, $\mathbf{C} < \mathbf{D}$, $[I]$ decreasing, $\langle k \rangle$ decreasing,
4. $\mathbf{A} < \mathbf{B}$, $\mathbf{C} > \mathbf{D}$, $[I]$ decreasing, $\langle k \rangle$ increasing.

5.2 Oscillation of the network structure

While some studies focusing on adaptive or dynamic networks consider and analyse changes in network structure, a large proportion of papers either only or mainly focus

on system level quantities such as infectious prevalence or some other population level indicator with the main aim of characterising this via a bifurcation theory type analysis. It has been observed that the networks themselves can also undergo significant changes in time for appropriate parameter combinations and values. For example, the segregation of networks into different components has been observed by Gross et al. (2006), and see Fig. 8. Such analysis can reveal important network features which can invalidate the use of mean-field or pairwise models and, more importantly, may reveal the impact of the interplay between dynamics on and of the network. The emergence of network structure from such dynamic network models could be also interpreted as a more natural or organic emergence of structure, as opposed to artificial or synthetic network models.

The most interesting types of networks or network properties that emerge from our model are: (a) networks with bimodal-like degree distribution and (b) networks where the largest connected component does not contain all nodes. These are observed at crucial or turning points along the oscillatory cycle of the epidemic. Namely, bimodal-like degree distributions are a feature of the network at low infection prevalence level when the susceptible and infected nodes segregate with few inter-component links. Here, link creation will increase the density in the susceptible cluster, while link cutting thins connections between infected nodes. Similarly, and also around this point, the clumping of similar states together, see Fig. 8c and d leads to the network being composed of multiple disjoint components. Networks with these properties can be repeatedly observed at the corresponding points along the oscillatory cycle. In the growing stages of the epidemic, as well as at the peak of it, networks are generally close to random or Erdős-Rényi type networks.

5.3 Exact master equation

In order to understand the behaviour of the system we consider the exact master equations. First, let us describe the state space. Let N denote the number of nodes and $E = N(N-1)/2$ the maximum number of edges. Fixing a network, the total number of states is 2^N since each node can be either an S or an I node. Each edge can be switched on or switched off, hence the total number of networks on N nodes is 2^E. For each network we have 2^N states, hence there are 2^{N+E} states in the state space. Even for small values of N the state space becomes extremely large. For the sake of clarity however, the simplest cases of $N = 2$ and $N = 3$, i.e., for dynamic graphs with two or three nodes, are illustrated in Appendix B. For the case $N = 2$, the transition matrix M is also determined. This matrix has 2^{N+E} rows and columns and contains the transition probabilities between all possible states.

The master equation, describing the full system behaviour, takes the form $\dot{x}(t) = Mx(t)$, where x is the vector containing all attainable networks with all possible node labelings on them. For example, for a network on two nodes and with nodes labeled S or I, there are eight possible states $\{SS, SI, IS, II, \overline{SS}, \overline{SI}, \overline{IS}, \overline{II}\}$ and these give rise to an 8-dimensional vector $x(t)$, where $x_i(t)$ denotes the probability of the system being in the ith state at time t, see Appendix B for full details. Considering the special cases of small networks one can observe that this transition matrix has

a special structure, however, we do not study this structure in detail. Instead, we turn to the question of the presence of oscillations in this exact model. In order to answer this question the spectrum of the matrix M has to be studied. It is known that for any transition matrix the spectrum is in the left half of the complex plane and zero is an eigenvalue. The eigenvector corresponding to the zero eigenvalue has non-zero coordinates only at those system states where all nodes are susceptible, and these states form an absorbing set. In the case of $N = 2$ this eigenvector is $(\omega_{SS}, 0, 0, 0, \alpha_{SS}, 0, 0, 0)^T$. In the absorbing state all nodes are susceptible and the network changes dynamically according to the values of ω_{SS} and α_{SS}. The solution $x(t)$ of the master equation is a linear combination of functions of the form $e^{\lambda t}u$, where λ is an eigenvalue and u is an eigenvector of M. If $\lambda \neq 0$, then it has a negative real part, hence this function tends to zero as $t \to \infty$, that is, for large t only the absorbing state will be observed. However, typically there are eigenvalues with real part very close to zero yielding long time behaviour different from the absorbing state. For static networks these eigenvalues are real, hence the long time behaviour corresponds to a so-called quasi steady state, i.e., the expected prevalence is maintained at a non-zero constant value for a relatively long time. For dynamic networks this eigenvalue may be complex leading to damped oscillations, where slow damping leads to sustained, long-time oscillations.

Let us investigate briefly what sort of eigenvalues may be responsible for these oscillations. If the eigenvalue is complex, i.e., $\lambda = -\mu + i\nu$, then the dominant term in the expression of the prevalence is of the form $e^{-\mu t}\sin(\nu t)$, together with a similar term containing cosine instead of sine. A simple calculation shows that the ratio of two consecutive maxima is $\exp(-\mu/\nu)$. This ratio is always less than one showing that the oscillation is always damped, however, when μ/ν is small then this damping is getting smaller. The key question is how the magnitude or smallness of this ratio depends on the values of the parameters. Even though this question is far beyond the scope of this paper, we mention a general, classical result related to this problem. In the early forties of the last century Kolmogorov posed the following problem. If M is an $n \times n$ transition matrix of a continuous time Markov chain, find the location of its spectrum in the complex plane. Dmitriev and Dynkin proved that the spectrum is in the cone given by two half lines starting at the origin and having an angle $\frac{\pi}{2} - \frac{\pi}{n}$ with the negative part of the real axis (Dmitriev and Dynkin 1945). This implies that $\frac{\mu}{\nu} \geq \tan(\frac{\pi}{n})$. It is easy to show that there exists a matrix M for which equality can be achieved, i.e., there is a matrix that is optimal from the view point of oscillations. This matrix has ones below the diagonal and in the right top corner. This corresponds to a Markov chain with transitions aligned around a perfect cycle, thus giving rise to an idealised, perfect oscillator. The spectrum of our matrix M in the master equation is in a much narrower cone, meaning that it yields much more markedly damped oscillations.

Future work will seek to estimate the angle of the smallest cone containing the spectrum of M, as given by the dynamic network model. Intuitively, it seems that the bigger the angle is, the longer the cycles of the Markov chain are. We note that in the case of $N = 2$, for appropriate parameter combination, the longest cycle in the Markov chain's full transition diagram, see Fig. 9, has length four but with many potential perturbations or opportunities to deviate from the cycle (the cycle with length four is

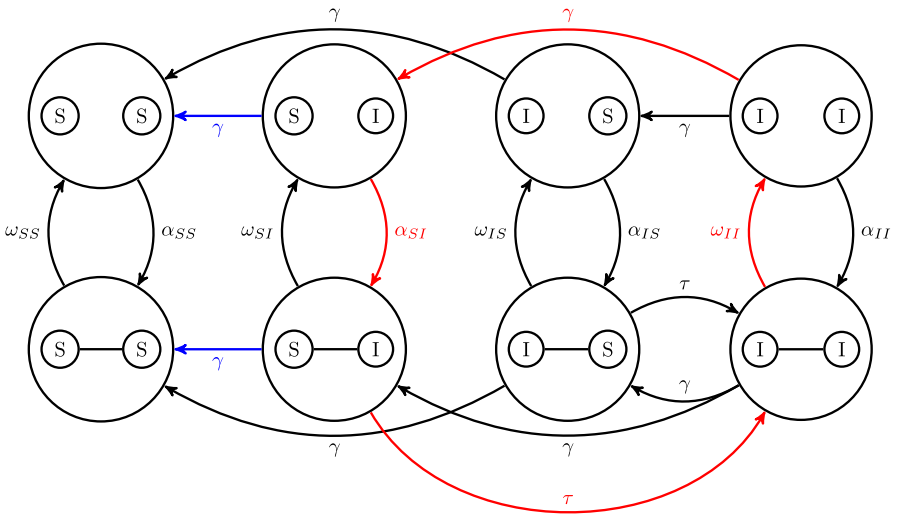

Fig. 9 The state space and the transitions for a dynamic network with two nodes. *Red arrows* represent the longest possible cycle of length four, with the *blue arrows* highlighting transitions that would drive the process off cycle (colour figure online)

highlighted by red arrows and the deviating transitions are shown by blue arrows in the figure). Summarising, we conjecture that the cycles in the Markov Chain's transition diagram are responsible for the oscillations observed in the probabilities of the states and in the expected values of some chosen quantities. Moreover, we claim that in the case of epidemic propagation in dynamic networks the Markov Chain's full transition map must contain cycles, with longer cycles and fewer potential off-cycles movements leading to stronger and more sustained oscillations.

6 Discussion

We proposed a dynamic network model using SIS epidemic propagation with preferential, i.e., link-type-based link activation and deletion. We analysed the pairwise model and carried out network-based stochastic simulations. The oscillations developing in the system were studied using Fourier analysis, as well as through analysing the exact stochastic model in terms of the master equations.

Both simple pairwise and compact pairwise models fail to accurately describe the oscillatory regime. One of the main reasons of this failure is that the closures in these systems are based on the assumption that the distribution of infected nodes around susceptible nodes is binomial, which does not hold in simulation, especially close to the die-out regime. Figure 8c, where infected and susceptible clumps are developed, clearly shows that the binomial assumptions is completely inaccurate. The poor performance of pairwise models for adaptive networks is known in the literature, see for example (Demirel et al. 2014). Further investigation of the time dependence of the network structure and the failure of the binomial assumption may reveal the reasons behind this phenomenon.

Other important questions worth mentioning are related to characterising and measuring changes in the structure or bifurcation of networks. For example, in Taylor et al. (2012), the connectedness of the network plays an important role in determining the outcome of the epidemic. However, one can choose to investigate the degree distribution or its average, and these may turn out to be more informative. For example, for our model and the choice of parameters, apart from considering the evolution of the average degree, one could potentially map out the evolution of clustering and that of the degree distribution. Indeed, the latter undergoes interesting changes from binomial-like to markedly bimodal when the network is close to the segregation point. These scenarios could be further investigated using the compact pairwise model in order to shed light on the evolution of the degree distribution, and could be used as a precursor to a more detailed analysis based on simulations. Clearly, there are many possibilities and the right choice may not be universal but model-dependent. Nevertheless, we wish to emphasise the importance of precisely describing changes in network structure, because it can then lead to a better understanding of how networks with certain properties emerge and why mean-field models break down.

Studying small toy networks and in particular the structure of the transition diagram of full Markov Chains, has allowed us to relate the oscillatory phenomena to cycles and their length in the Markov Chains. From our simple experiments, it is worth noting that the creation of II links, i.e., non-zero value of α_{II}, may lead to more pronounced oscillations, as this can lead to the appearance of longer cycles in the transition diagram. Finally, determining the transition diagram of the lumped systems for small graphs and investigating the maximal length of cycles in the transition portrait of the Markov Chain and their relation to the oscillations produced by the system could shed further light behind how oscillations emerge and can be sustained.

Acknowledgments Péter L. Simon acknowledges support from the Hungarian Scientific Research Fund (OTKA) (Grant No. 81403).

Compliance with ethical standards The authors declare that no conflict of interest exists. The Hungarian Scientific Research Fund (OTKA) had no role in study design, data analysis, decision to publish, or preparation of the manuscript. The work did not involve any human or animal research or data.

Appendix A: Bifurcation analysis of the mean-field model

In this appendix the steady states of system (1)–(4) and their stability is studied.

A1: Endemic steady state

The steady states are given by system (1)–(4) by putting zeros in the left hand sides (and omitting those parameters that are assumed to be zero), i.e. by system

$$0 = \tau[SI] - \gamma[I], \tag{8}$$

$$0 = \gamma([II] - [SI]) + \tau([SSI] - [ISI] - [SI]) - \omega_{SI}[SI], \tag{9}$$

$$0 = -2\gamma[II] + 2\tau([ISI] + [SI]), \tag{10}$$

$$0 = 2\gamma[SI] - 2\tau[SSI] + \alpha_{SS}([S]([S] - 1) - [SI]) \tag{11}$$

where the closures

$$[SSI] = \frac{(k_S - 1)[SS][SI]}{k_S[S]} \quad \text{and} \quad [ISI] = \frac{(k_S - 1)[SI][SI]}{k_S[S]} \tag{12}$$

are used with

$$k_S = \frac{[SS] + [SI]}{[S]}.$$

For simplicity, the steady state values of the four variables are denoted here by $[I]$, $[SI]$, $[II]$ and $[SS]$. All of them will be expressed in terms of $[S]$ and then a quartic equation for $[S]$ will be derived. It is obvious that $[I] = N - [S]$, then from (8) we get $[SI] = \frac{\gamma}{\tau}[I]$. Multiplying (9) by 2 and adding it to (10) and to (11) one can express $[SS]$ in terms of $[I]$ and $[S]$ as

$$[SS] = [S]([S] - 1) - 2\frac{\omega_{SI}\gamma}{\alpha_{SS}\tau}[I]. \tag{13}$$

From (10) we can express $[II]$ in terms of $[I]$ and $[S]$ as

$$[II] = \frac{\tau[SI]}{\gamma}\left(\frac{[SI]}{[S]} - \frac{[SI]}{[SS] + [SI]} + 1\right). \tag{14}$$

Multiplying (9) by 2 and adding it to (10) we get

$$2\tau[SSI] - 2\gamma[SI] - 2\omega_{SI}[SI] = 0.$$

Using the closure and dividing by $2[SI]$ yields

$$\frac{[SS]}{[S]} - \frac{[SS]}{[SS] + [SI]} = \frac{\gamma + \omega_{SI}}{\tau}.$$

Now substituting $[SI] = \frac{\gamma}{\tau}(N - [S])$ and (13) into this equation one obtains the following quartic equation for $x = [S]$

$$x^4 + A_3x^3 + A_2x^2 + A_1x + A_0 = 0 \tag{15}$$

with

$$\begin{aligned}
A_3 &= 4ab - 3 - 2b - c \\
A_2 &= 2 + 2b + c + b^2 + bc - 6ab - 4ab^2 - 2abc + 4a^2b^2 + Nb(1 - 4a) \\
A_1 &= Nb(-1 + 6a - b - c + 6ab + 2ac - 8a^2b) \\
A_0 &= 2N^2ab^2(1 - 2a),
\end{aligned}$$

where $a = \frac{\omega_{SI}}{\alpha_{SS}}$, $b = \frac{\gamma}{\tau}$ and $c = \frac{\omega_{SI}}{\tau}$.

Once (15) is solved for x, then the steady state ($[I]$, $[SI]$, $[II]$, $[SS]$) is given by $[I] = N - x$, $[SI] = \frac{\gamma}{\tau}[I]$, (13) and (14). A solution x yields a biologically meaningful steady state if all of its coordinates are non-negative. An extensive numerical study showed that for any combination of the parameters there can be at most one endemic steady state. The endemic steady state exists if the disease-free equilibrium is unstable. The condition for that is determined in the next subsection. We note that the above calculation yields only the endemic steady states because during the derivation of the quartic equation there was a division by $2[SI]$, which is zero at the disease-free steady state.

A2: Stability of the disease-free steady state

The stability of the disease-free steady state is determined by the Jacobian matrix determined at $([I], [SI], [II], [SS]) = (0, 0, 0, N(N-1))$. In order to compute this matrix we determine the partial derivatives of the triples at this steady state, as they are given by the closures (12).

$$\frac{\partial[SSI]}{\partial[I]} = 0, \quad \frac{\partial[SSI]}{\partial[SI]} = N-2, \quad \frac{\partial[SSI]}{\partial[II]} = 0, \quad \frac{\partial[SSI]}{\partial[SS]} = 0,$$
$$\frac{\partial[ISI]}{\partial[I]} = 0, \quad \frac{\partial[ISI]}{\partial[SI]} = 0, \quad \frac{\partial[ISI]}{\partial[II]} = 0, \quad \frac{\partial[ISI]}{\partial[SS]} = 0,$$

Using these partial derivatives the Jacobian matrix at the disease-free steady state can be given as

$$J = \begin{pmatrix} -\gamma & \tau & 0 & 0 \\ 0 & -\gamma + \tau(N-2) - \tau - \omega_{SI} & \gamma & 0 \\ 0 & 2\tau & -2\gamma & 0 \\ \alpha_{SS}(1-2N) & 2\gamma - 2\tau(N-2) & 0 & -\alpha_{SS} \end{pmatrix}.$$

It can be easily seen that $-\alpha_{SS}$ and $-\gamma$ are eigenvalues of this matrix. The remaining two eigenvalues are the eigenvalues of the 2×2 matrix in the middle:

$$\begin{pmatrix} -\gamma + \tau(N-2) - \tau - \omega_{SI} & \gamma \\ 2\tau & -2\gamma \end{pmatrix}.$$

The disease-free steady state is asymptotically stable if and only if all the eigenvalues have negative real part. This has to be checked only for the above 2×2 matrix. For a 2×2 matrix the eigenvalues have negative real part if and only if its determinant is positive and its trace is negative. The determinant is positive if $\gamma + \omega_{SI} - \tau(N-2) > 0$. The trace is positive if $3\gamma + \omega_{SI} - \tau(N-3) > 0$. The first condition implies the second one, hence we proved Proposition 1.

A3: Stability of the endemic steady state

The stability of the endemic steady state can be determined only numerically. For a given set of the parameters the coordinates of the endemic steady state can be computed according to Appendix A1. The partial derivatives in the Jacobian J can be calculated analytically, then substituting the numerically obtained coordinates of the endemic steady state we get the entries of the Jacobian numerically. This enables us to calculate the coefficients of the characteristic polynomial

$$\lambda^4 - b_3\lambda^3 + b_2\lambda^2 - b_1\lambda + b_0,$$

where $b_3 = \mathrm{Tr}\, J$, $b_0 = \det J$ and b_1, b_2 can be given as the sum of some subdeterminants of the Jacobian, the concrete form of which is not important at this moment. To find the parameter values where Hopf bifurcation occurs we use the method introduced in Szabó et al. (2012). In the case of 4×4 matrices the necessary and sufficient condition for the existence of pure imaginary eigenvalues is

$$b_0 b_3^2 = b_1(b_2 b_3 - b_1) \quad \text{and} \quad \operatorname{sign} b_1 = \operatorname{sign} b_3, \tag{16}$$

These relations will be considered here as necessary conditions for the Hopf-bifurcation. The transversality conditions will not be checked because of their complexity; instead, parameter values on the two sides of the bifurcation curve are chosen and the behaviour of the corresponding systems is checked numerically, to show that a Hopf-bifurcation really occurs along that curve. The Hopf-bifurcation set in the (τ, ω_{SI}) parameter plane can be obtained as follows. For a given value of τ we compute the value of $b_0 b_3^2 = b_1(b_2 b_3 - b_1)$ numerically as ω_{SI} is varied. It turns out that for a range of τ values this expression changes sign twice as ω_{SI} is varied. More precisely, for given values of the other parameters (N, γ, α_{SS}) there exist τ values τ_1 and τ_2, such that for $\tau \in (\tau_1, \tau_2)$ we get ω_1 and ω_2 such that for $\omega_{SI} = \omega_i$ $(i = 1, 2)$ we have $b_0 b_3^2 = b_1(b_2 b_3 - b_1)$, i.e. Hopf bifurcation occurs at $\omega_{SI} = \omega_i$ $(i = 1, 2)$. If τ is not in the interval (τ_1, τ_2), then there is no Hopf bifurcation, i.e., the relation $b_0 b_3^2 = b_1(b_2 b_3 - b_1)$ cannot hold. For $\tau \in (\tau_1, \tau_2)$ and $\omega_{SI} \in (\omega_1, \omega_2)$ there is a stable periodic orbit. If ω_{SI} is outside the interval (ω_1, ω_2), then there is no periodic orbit and either the endemic or the disease-free steady state is stable. The final state of the system is shown in the bifurcation diagram in Fig. 1.

Appendix B: State space and transition matrix for adaptive graphs with $N = 2$ and $N = 3$

In the case $N = 2$, i.e., for a graph with two nodes, the number of edges is at most $E = 1$. That is there are two graphs on two nodes, one is a single edge the other one consists of two disjoint nodes. We denote the states with $\{SS, SI, IS, II\}$ when the graph consists of two disjoint nodes. Here the state SI means that node 1 is S and node 2 is I. The states are denoted by $\{\overline{SS}, \overline{SI}, \overline{IS}, \overline{II}\}$ when the graph is a single edge. Thus the full state space for $N = 2$ contains the following 8 states:

$\{SS, SI, IS, II, \overline{SS}, \overline{SI}, \overline{IS}, \overline{II}\}$. Consider now the transitions between these states. There are two types of transitions: epidemic transitions (infection and recovery) and network transitions (creating and deleting edges). Epidemic transitions may occur among states that belong to the same graph, that is within the subsets $\{SS, SI, IS, II\}$ and $\{\overline{SS}, \overline{SI}, \overline{IS}, \overline{II}\}$. Within the first subset only recovery may occur since these states belong to a graph that consists of two separate nodes. So the only possible transitions are $SI \to SS$, $IS \to SS$, $II \to IS$ and $II \to SI$, these may happen with rate γ. Within the subset $\{\overline{SS}, \overline{SI}, \overline{IS}, \overline{II}\}$ infection may happen as well, hence the possible transitions are $\overline{SI} \to \overline{II}$ and $\overline{IS} \to \overline{II}$ with rate τ and $\overline{SI} \to \overline{SS}$, $\overline{IS} \to \overline{SS}$, $\overline{II} \to \overline{IS}$ and $\overline{II} \to \overline{SI}$ with rate γ. Network transitions occur between states in which the corresponding nodes are of the same type. For example, the transition $SS \to \overline{SS}$ occurs at rate α_{SS} since an SS type edge is created during this transition. Similarly, the transition $\overline{SS} \to SS$ occurs at rate ω_{SS} since an SS type edge is deleted during this transition. In general, the transition $AB \to \overline{AB}$ happens at rate α_{AB} and the transition $\overline{AB} \to AB$ happens at rate ω_{AB}, where $A, B \in \{S, I\}$. All the transitions are shown in Fig. 9. If the states are ordered as $\{SS, SI, IS, II, \overline{SS}, \overline{SI}, \overline{IS}, \overline{II}\}$, then the transition matrix of the corresponding Markov chain takes the form

$$M = \begin{pmatrix} M_{11} - A & \Omega \\ A & M_{22} - \Omega \end{pmatrix},$$

where

$$M_{11} = \begin{pmatrix} 0 & \gamma & \gamma & 0 \\ 0 & -\gamma & 0 & \gamma \\ 0 & 0 & -\gamma & \gamma \\ 0 & 0 & 0 & -2\gamma \end{pmatrix}, \quad M_{22} = \begin{pmatrix} 0 & \gamma & \gamma & 0 \\ 0 & -\tau - \gamma & 0 & \gamma \\ 0 & 0 & -\tau - \gamma & \gamma \\ 0 & \tau & \tau & -2\gamma \end{pmatrix},$$

$$A = \begin{pmatrix} \alpha_{SS} & 0 & 0 & 0 \\ 0 & \alpha_{SI} & 0 & 0 \\ 0 & 0 & \alpha_{SI} & 0 \\ 0 & 0 & 0 & \alpha_{II} \end{pmatrix}, \quad \Omega = \begin{pmatrix} \omega_{SS} & 0 & 0 & 0 \\ 0 & \omega_{SI} & 0 & 0 \\ 0 & 0 & \omega_{SI} & 0 \\ 0 & 0 & 0 & \omega_{II} \end{pmatrix}.$$

The matrices M_{11} and M_{22} contain the transition rates corresponding to the epidemic transitions. These rates belong to the transitions within the subsets $\{SS, SI, IS, II\}$ and $\{\overline{SS}, \overline{SI}, \overline{IS}, \overline{II}\}$, respectively. The matrices A and Ω contain the network transition rates that correspond to transitions between these two subsets. The master equation can be written as $\dot{x}(t) = Mx(t)$, where the coordinates of the eight dimensional vector $x(t)$ are the probabilities of the states at time t.

Let us briefly consider the case $N = 3$. Then $E = 3$, hence there are $2^3 = 8$ different possible graphs, one without any edges, three graphs with one edge, three line graphs with two edges and a triangle with three edges. Each graph can be in 8 possible states, namely $\{SSS, SSI, SIS, ISS, SII, ISI, IIS, III\}$. Hence there are $2^3 \cdot 2^3 = 64$ states altogether. Epidemic transitions may occur among states that belong to the same graph, for example, in the case of a triangle graph the transition $IIS \to III$ happens at rate 2τ, while its rate is τ for a line graph where node 2 is connected to node

1 and node 3. The transition rate may be zero, e.g., in the case when there is only one edge in the graph connecting nodes 1 and 2, or in the case when there are no edges at all in the graph. Network transitions occur between states in which the corresponding nodes are of the same type. For example, denoting by SSS the state where all nodes are susceptible and the graph consist of three disjoint nodes, and by $\overline{SS}S$ the state where all nodes are susceptible and the graph contains one edge that connects node 1 and 2, the rate of transition $SSS \to \overline{SS}S$ is α_{SS}, while the rate of transition $\overline{SS}S \to SSS$ is ω_{SS}. The master equations take again the form $\dot{x}(t) = Mx(t)$, where the coordinates of the 64-dimensional vector $x(t)$ are the probabilities of the states at time t.

We note that the size of the state space can be reduced by lumping some states together, similarly to the case of static graphs (Simon et al. 2010). The lumping of the state space for dynamic network processes is beyond the scope of this paper, here we only mention a few simple cases where lumping can be carried out. In the case $N = 2$ it is easy to see that the states SI and IS can be lumped together, which means that their sum can be introduced as a new variable, and their differential equations can be added up. Similarly, the sum of $\overline{SI}$ and $\overline{IS}$ can be introduced as a new variable. (By adding their differential equations one can immediately see that the old variables will not appear in the remaining system of equations). Hence the eight-dimensional system $\dot{x}(t) = Mx(t)$ can be reduced to a six-dimensional system by lumping. In the case $N = 3$ we have even more chance for lumping if it is assumed that $\alpha_{SI} = 0$, $\alpha_{II} = 0$, $\omega_{SS} = 0$, $\omega_{II} = 0$. Without explaining the details we claim that in this case the 64-dimensional system of master equations can be reduced to a 20-dimensional one by lumping. In the case $N = 4$ the dimension of the state space can be reduced from 1024 to 89.

References

Demirel G, Vazquez F, Böhme GA, Gross T (2014) Moment-closure approximations for discrete adaptive networks. Phys D Nonlinear Phen 267:68–80

Dmitriev N, Dynkin E (1945) On the characteristic roots of stochastic matrices. C R (Dokl) Acad Sci URSS 49:159–162

Eames KTD, Keeling MJ (2002) Modeling dynamic and network heterogeneities in the spread of sexually transmitted diseases. Proc Natl Acad Sci USA 99:13330–13335

Gillespie DT (1976a) A general method for numerically simulating the stochastic time evolution of coupled chemical reactions. J Comput Phys 22:403–434

Gillespie DT (1976b) Exact stochastic simulation of coupled chemical reactions. J Phys Chem 81:2340–2361

Gross T, D'Lima CJD, Blasius B (2006) Epidemic dynamics on an adaptive network. Phys Rev Lett 96:208701

Gross T, Kevrekidis IG (2008) Robust oscillations in SIS epidemics on adaptive networks: coarse graining by automated moment closure. Euro Phys Lett 82:38004

Gross T, Blasius B (2008) Adaptive coevolutionary networks: a review. J R Soc Interface 5:259–271

Halliday DM, Rosenberg JR, Amjad AM, Breeze P, Conway BA, Farmer SF (1995) A framework for the analysis of mixed time series/point process data-theory and application to the study of physiological tremor, single motor unit discharges and electromyograms. Prog Biophys Mol Biol 64:237–278

House T, Keeling MJ (2011) Insights from unifying modern approximations to infections on networks. J R Soc Interface 8:67–73

Juher D, Ripoll J, Saldaña J (2013) Outbreak analysis of an SIS epidemic model with rewiring. J Math Biol 67:411–432

Keeling MJ (1999) The effects of local spatial structure on epidemiological invasions. Proc R Soc Lond B 266:859–867

Kiss IZ, Berthouze L, Taylor TJ, Simon PL (2012) Modelling approaches for simple dynamic networks and applications to disease transmission models. Proc R Soc A 468(2141):1332–1355

Marceau V, Noël PA, Hébert-Dufresne L, Allard A, Dubé LJ (2010) Adaptive networks: coevolution of disease and topology. Phys Rev E 82:036116

Rogers T, Clifford-Brown W, Mills C, Galla T (2012) Stochastic oscillations of adaptive networks: application to epidemic modelling. J Stat Mech 2012:P08018

Sayama H, Pestov I, Schmidt J, Bush B, Wong C, Yamanoi J, Gross T (2013) Modeling complex systems with adaptive networks. Comput Math Appl 65:1645–1664

Shaw LB, Schwartz IB (2008) Fluctuating epidemics on adaptive networks. Phys Rev E 77:066101

Simon PL, Taylor M, Kiss IZ (2010) Exact epidemic models on graphs using graph automorphism driven lumping. J Math Biol 62:479–508

Szabó A, Simon PL, Kiss IZ (2012) Detailed study of bifurcations in an epidemic model on a dynamic network. Differ Equ Appl 4:277–296

Taylor M, Taylor TJ, Kiss IZ (2012) Epidemic threshold and control in a dynamic network. Phys Rev E 85:016103

Zhou J, Xiao G, Cheong SA, Fu X, Wong L, Ma S, Cheng TH (2012) Epidemic reemergence in adaptive complex networks. Phys Rev E 85:036107